Analysis of the magnet support structure for the plasma fusion experiment Wendelstein 7-X

Nikola Jaksic [a,*], Paul van Eeten [b], Victor Bykov [b], Felix Schauer [b]

[a] Max-Planck-Institute for Plasma Physics, EURATOM Association, Engineer/Scientist, Boltzmannstraße 2, D-85748 Garching, Germany
[b] Max-Planck-Institute for Plasma Physics, EURATOM Association, Engineer/Scientist, Branch Institute Greifswald, Germany

ARTICLE INFO

Article history:
Available online 23 November 2010

Keywords:
Plasma fusion
Stellerator experiment
Superconducting coils
FE analysis

ABSTRACT

The world's largest plasma fusion experimental device of the stellarator family named Wendelstein 7-X (W7-X) [http://www.ipp.mpg.de/ippcms/eng/for/projekte/w7x/index.html] is being built at the Max-Planck-Institute for Plasma Physics (IPP) in Greifswald, Germany. The mission of the experiment is to prove the fusion reactor relevance of the stellarator principle [1,2].

Main subject of this paper is the description of the numerical simulation of the highly complex and multiple nonlinear W7-X magnet system structure with the code ADINA. This code was chosen right from the start of the project and has later been used in parallel with the subsequently installed ANSYS and ABAQUS codes until now.

The ADINA W7-X global structure model is the result of a long term R&D work on the superconducting coils and related support structure optimization. Despite the fact that W7-X is already in the assembly phase, there are still large structural analysis efforts going on. Their aim is to accompany the machine construction by evaluating specific assembly issues, non-conformities and design changes, but also to evaluate the operational limits of the experimental device which in many respects is an absolute prototype worldwide.

1. Introduction

Plasma fusion research projects are established with the objective of producing energy by fusion of the ionized hydrogen isotopes deuterium and tritium in very hot plasmas. W7-X is an experimental device of the stellarator type which is based on the magnetic plasma confinement principle. The R&D activities on the present structural system of the experimental device were carried out over a period of over 18 years. The main steps of the R&D activities are published in [3–9].

This paper focuses on some remarkable issues like complex FE model structuring and benchmarking with alternative models in different codes and highlights some experience which might be relevant also for other large structures with high complexity. Finally an analyses comparison of the same FE model with two different finite element orders is considered.

The main structural components of the five-periodic toroidal device are the magnet system, the cryostat (plasma and outer vessels, ports) and the machine base (Fig. 1). The plasma vessel closely follows the twisted shape of the plasma. The outer vessel and the plasma vessel are penetrated by about 250 ports. The ports with different forms (round, elliptic, rectangular) provide access to the plasma vessel interior for maintenance, supply and plasma diagnostic. Table 1 shows a summary of the experimental device characteristic data.

The superconducting magnet system (Fig. 2) is surrounded by the plasma vessel at the inside and the outer vessel on the outside. The whole magnet structure is kept at a cryogenic temperature of $\sim$4 K and in a high vacuum of $\sim 10^{-4}$ Pa. The superconducting magnet system with its support structure is the main subject of the considerations.

Important characteristics of the magnet geometry are the five-fold symmetry and the modularity of the coil arrangement system. The axes of symmetry in Fig. 2 are denoted by the characters A1 to A5 for the major, and B1 to B5 for the minor axes. The coil system consists of 50 modular field coils (MF) and 20 ancillary field coils (AF). Due to symmetry conditions only five MF and two AF coil types exist, all of them arranged within one of the ten half-modules each. The toroidal coil system has an average large diameter of 11 m. The MF coils are wound with six, the AF coils with three double layers of a cable in conduit conductor which is cooled by forced

* Corresponding author. Tel.: +49 89 32991134; fax: +49 89 32991620.
E-mail address: nikola.jaksic@ipp.mpg.de (N. Jaksic).

0045-7949/$ - see front matter © 2010 Elsevier Ltd. All rights reserved.
doi:10.1016/j.compstruc.2010.10.017

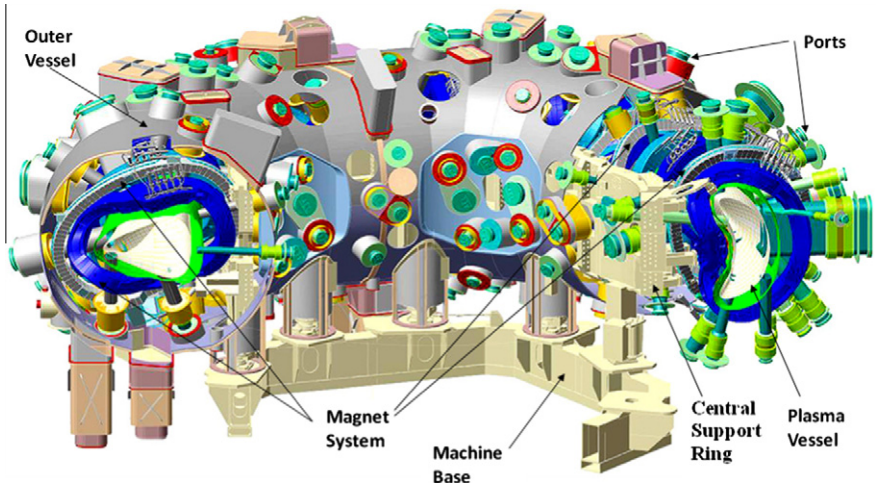

Fig. 1. Main structural components.

Table 1
Characteristic data of W7-X experimental device.

Machine diameter	15 m
Total height	4 m
Weight	550 ton
Major plasma radius	5.5 m
Minor average plasma radius	0.53 m
Plasma volume	30 m
Number of non-planar coils	50
Number of planar coils	20
Magnetic field on the axis	3 T
Magnetic field at coil winding pack	6.7 T (non-planar coil)
Plasma pulse length	10 s at full heating power

flow supercritical helium at a temperature of ~4 K. An assembly of a MF coil is shown in Fig. 3.

Each individual coil housing is fully separated from the others (Fig. 4) and has to carry the primary load caused by electromagnetic forces. The coil housings are fixed to the central support ring with special joints called "central support elements" (CSE) at two locations only. Additionally, mutual support between adjacent coil housings is realized by intermediate joints which are mainly loaded by compressive loads. These intermediate joints (located at different positions at the circumference of the coils) are operating with different functions: At the regions where the distances between the coils are small (inboard segment of the coil housing) "narrow support elements" (NSE), realized by sliding contact elements, are balancing the compressive forces between two adjacent coils.

Other fixed intermediate joints, so called "lateral support elements" (LSE), are installed at the outboard side of the coils. They support also tension and shear forces. The AF coils are fixed laterally at both sides to the MF coils with so called planar support elements (PSE). These fixations are partly also realized using sliding contacts so that radial displacements (viewed in local coordinate system of the coil) are performed without constraints. Additional contact elements (CE), positioned at the top and bottom side of the MF coils in the half module symmetry surface, increase the

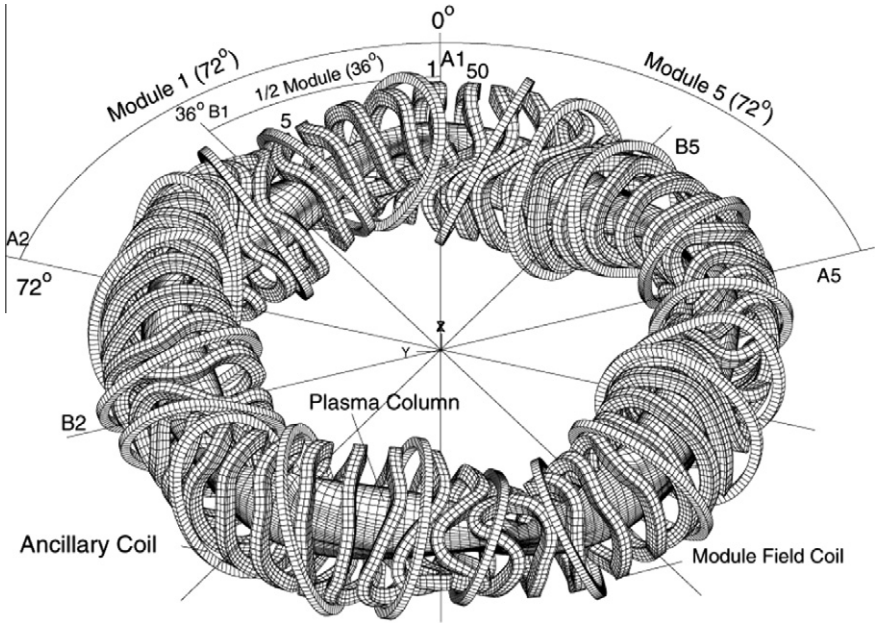

Fig. 2. Coil arrangement of W7-X with axes of symmetry.

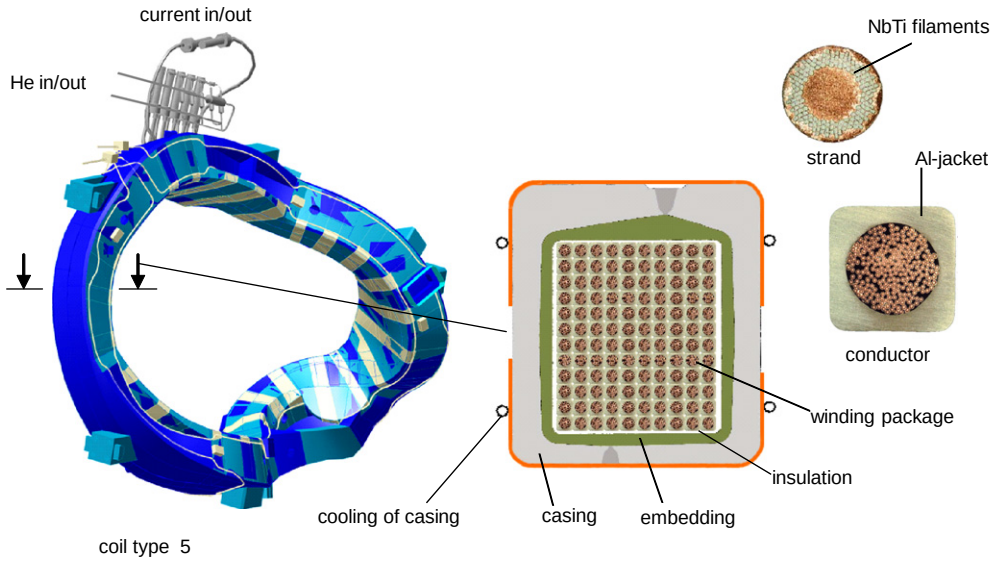

Fig. 3. Assembly of a superconducting magnet coil – W7-X.

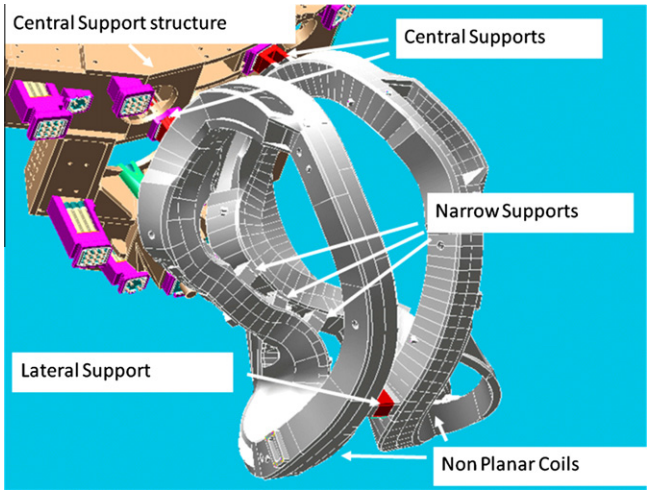

Fig. 4. Support structure for non-planar coils type three and four.

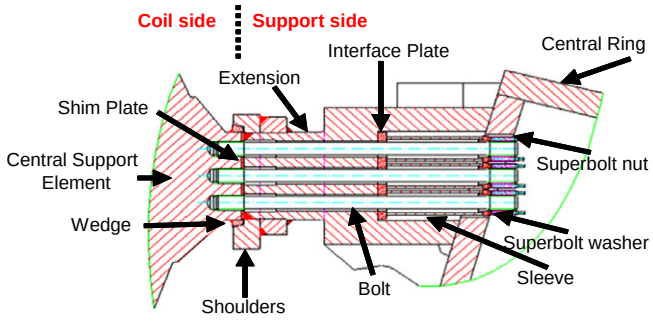

Fig. 5. Cross-section of a typical Central Support Extension with 3 × 3 bolt array.

lateral stiffness of the coil arrangement. The coil housing connections of the MF and AF coils to the support ring (via CSE) have been realized using bolted connections. Due to the complex geometry of the NSEs and LSEs and the enormous loads they have to withstand a special investigation for these structural parts was required.

The main constraints of the mechanical structure design are caused by the complexity of the geometry, the required small distance between the plasma and the non-planar coils in the inner region, the accuracy of the magnetic field, the high number of ports, and the limited access for assembly.

2. Support structure details

The most critical connection elements are the central support bolted connections, the narrow support sliding connections, and some lateral support connections. The central support connections are based on a "single central rod" or on a "matrix of rods" in Inconel 718. Part of these flange connections are allowed to open slightly so the rods need to be sufficiently long in order to maintain their strain values below the yield limit. A length section of a typical 3 × 3 bolt array is shown in Fig. 5. The inconel rods are screwed on welded blocks on the MF and AF coil casings and tightened through nuts and sleeves to extensions of the central ring.

In order to withstand the shear loads and the torsion moments acting on the central support extensions (CSE), shoulders are introduced on the central ring extensions to avoid relying only on friction. Shims and wedges are used between the coil blocks and shoulders in order to adjust accurately the coil positions.

The basic design of the narrow support elements (NSE) is shown in Fig. 6. A central pad made of Al-bronze is inserted between the stainless steel counter-faces located on the coil casing and the padframe of the opposite coil. The pad with a spherical surface can slide and tilt with respect to the stainless steel counter-faces and is protected from dust by a cap.

For smooth gliding of the pads on the counter-faces, both sides are coated with the low friction factor material MoS_2.

3. FE model description

3.1. Model modelling

The FE model development has been realized with PATRAN [10] code. Solid hexahedral 8 node finite elements have been used for

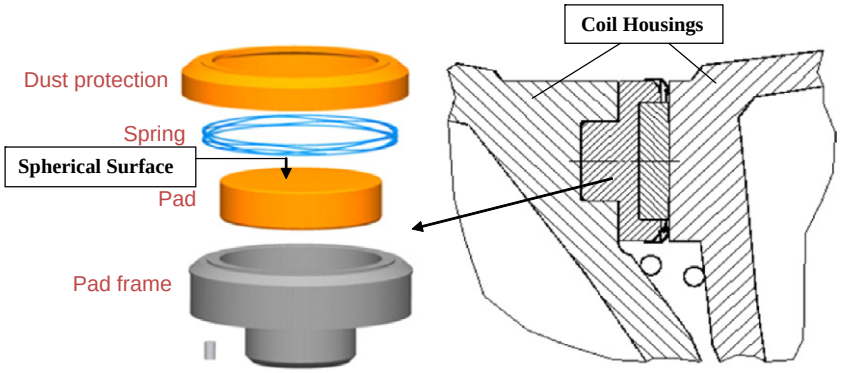

Fig. 6. Basic design of the narrow support elements.

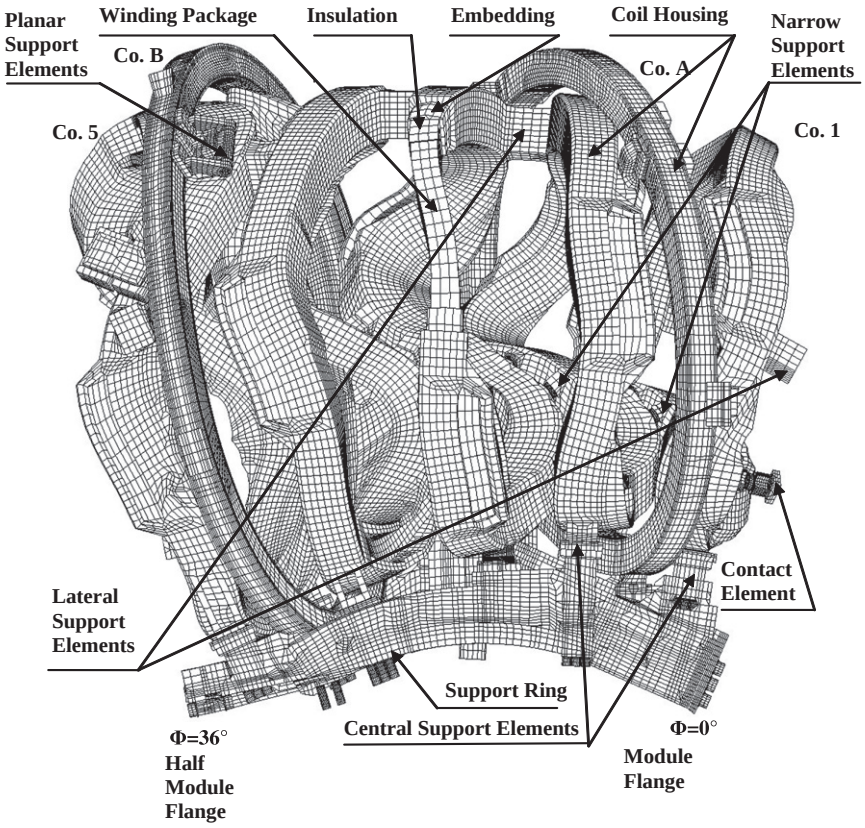

Fig. 7. FE model – top view.

the model definition at the beginning. The mesh constitution allowed an automatic update of the 8 node hexahedral finite elements to the 20/21 node elements. Among the hexahedral finite elements in some special cases a small number of wedge elements have been allowed. A small number of beam elements are used inside of the structure for modelling the bolts. 3-D contact surface elements have been used for the definition of the geometrical nonlinearities at e.g. NSEs and for all flanges inside of the structure. The finite elements quality and the geometry discretisation accuracy was a very important aspect during model generation. An average aspect-ratio of 1.5 without element distortion for all important partitions of the structure was intended. In general, the quality of the hexahedral elements has been controlled by shape features like edge angle and face skew which are kept under the threshold mark of 30.0° the face wrap under 7.0°, the face taper under 0.8 and the aspect ratio under 5.0. Also the discrepancies between FE mesh and original geometry in regions with complex geometry are within 1 mm.

All solid elements of the structure are meshed continuously. Because of the very complex and sensitive structure any glue of different mesh patterns inside of a solid has been avoided.

The FE model (Figs. 7 and 8) is reduced to 1/10th of the whole system (one half-module), consisting of five MF and two AF coils, by introducing special boundary conditions. This is possible because the original geometry as well as the loading of the structure obey specific symmetry properties. Table 2 shows a comparison of the main parameters for both models.

The derivation of the special symmetry definition with all restrictions is described in detail in [11]. Neglecting the influence of gravity, a 36° sector model can be built using these boundary

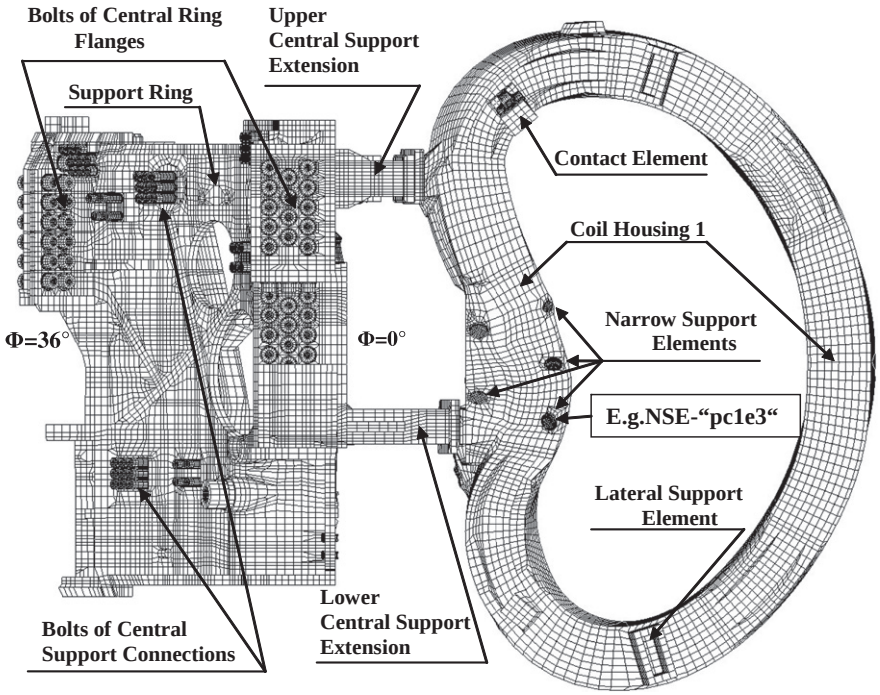

Fig. 8. Suspension of the coil casing 1 on the support ring – side view to the coil.

Table 2
FE model main parameters.

	8 node elements model	20 node elements model
Node number	368.369	1.331.737
Element number	249.775	249.775
Number of contact surfaces pairs	23	23
Number of contact surfaces	104	104
Number of contact segments	123.785	123.785
Degrees of freedom	1.688.991	5.865.765

conditions. Considering gravity, an extension to a 72° sector model has to be realized.

The coil winding pack is the core of the structure and also the origin for the definition of the FE mesh pattern and the mesh fineness. The coil winding pack is meshed by a subdivision of $3 \times 4 \times 96$ with the aim to build rectangular hexahedral element as far as possible. The first version of the coil winding pack includes 8 node hexahedral elements; an update possibility to 20 node hexahedral elements is warranted. The coil housing basic body is meshed by 8 node hexahedral elements. The mesh pattern includes 6 elements in the local lateral direction, eight elements in the local radial direction, 192 elements on circumference and one element for each corner. The mesh pattern mentioned above and only one element across the wall thickness warrant an element shape close to the rectangular solid. The update possibility to 20 node hexahedral elements with the view to check the accuracy of the results is included as well.

For modelling of both ancillary coil housings, complex mesh patterns were needed. These housings are assembled by bolts and additionally stiffened by pins at the edges. The number of bolts per coil edge is approximately 100 and of pins approximately 70.

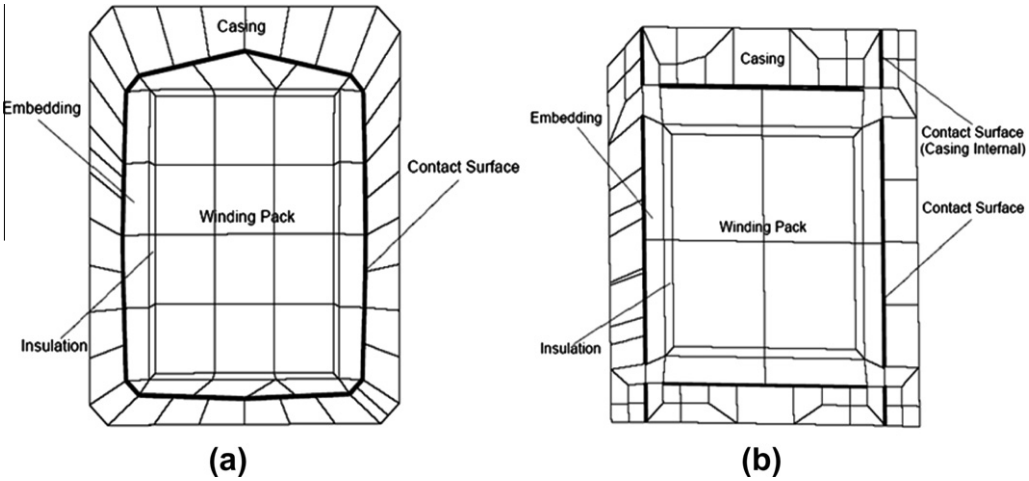

Fig. 9. Discretization of the coil cross-section – (a) MF coil and (b) AF coil.

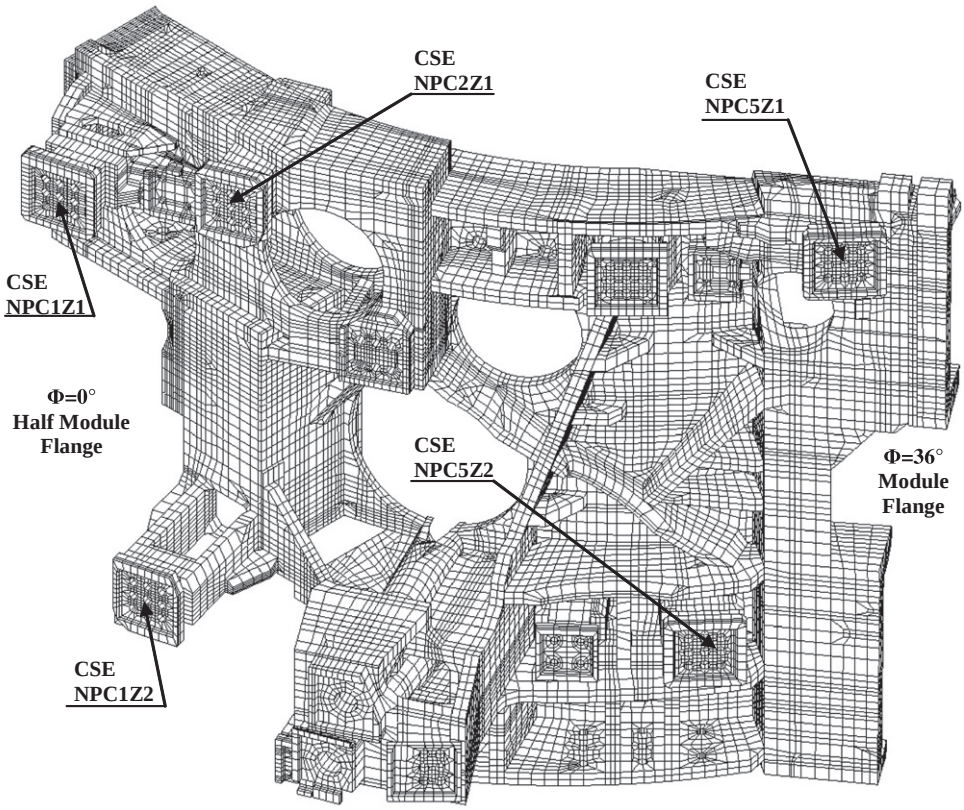

Fig. 10. Mesh of the central support ring – bird's eye view.

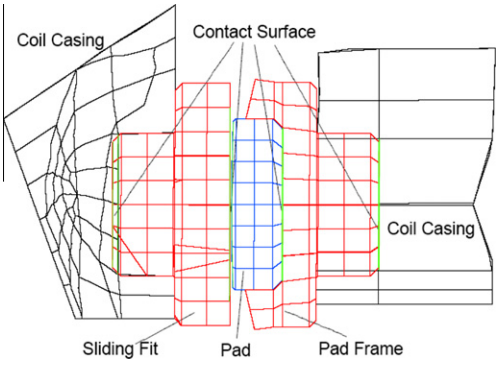

Fig. 11. Narrow support element (cross-section).

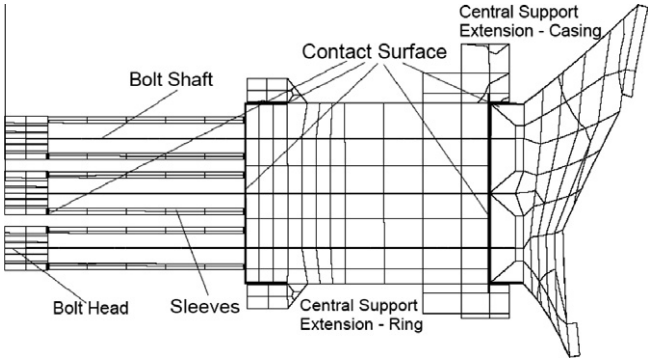

Fig. 12. Central support extension (cross-section).

Table 3
Material assignment.

Structural part	Material property
MF coil housing	Isotropic – Cast stainless steel 1.3690
AF coil housing	Isotropic – Stainless steel 1.4429
Central support ring	Isotropic – Cast stainless steel 1.3690/ Stainless steel 1.4429
Central support extensions	Isotropic – Cast stainless steel 1.3690/ Stainless steel 1.4429
Lateral support extensions	Isotropic – Stainless steel 1.4429
Narrow support elements – Pads	Isotropic – Al-Bronze
Bolts	Isotropic – Inconel 718
Coil winding pack	Orthotropic
Coil winding pack – Insulation	Orthotropic
MF coil winding pack – Embedding	Isotropic
AF coil winding pack – Embedding	Orthotropic

Their distribution around the circumference is in general irregular. In order to warrant the precise position of the bolts and pins within the planar coil casing, it was necessary to include this position coordinate values into the "meshing algorithm" as a condition.

Fig. 9(a) shows the discretisation of the MF coil cross-section and (b) shows the discretisation of the AF coil cross-section.

The central support ring (Fig. 10) is also fully meshed by hexahedral elements. Due to the fact that the central support ring is subjected to strong bending moments, the 20 node hexahedral elements are used right from the start of the analysis. The mesh of the remainder of the structure is adapted to the main part or to the local geometric conditions.

The most stressed parts of the structure like the narrow support elements or central support extensions are separated from the structure described above by contact surfaces and consequently

Table 4
Material properties.

Material name	Temp [K]	Density [kg/m^3]	Young's modulus [GPa]			Shear modulus [GPa]			Poisson's ratio [–]			Thermal expansion coefficient [10^{-6}/K]		
			X	Y	Z	XY	XZ	YZ	XY	XZ	YZ	X	Y	Z
Cast stainless steel 1.3690	4	7800		158					0.30				10.2	
	293	7800		148					0.30				10.2	
Stainless steel 1.4429	4	7800		197					0.28				10.38	
	293	7800		183					0.29				10.38	
Inconel 718	4	7800		204					0.30				8.06	
	293	7800		206					0.30				8.04	
Al-Bronze	4	7600		127					0.28				10.38	
	293	7600		113					0.28				10.38	
Embedding	4	2000		23.5					0.32				12.1	
	293	2000		10.3					0.34				12.1	
MF coil ground insulation	4	2000	22.0	31.0	37.0	6.7	10.6	6.7	0.21	0.18	0.23	13.7	6.9	4.6
	293	2000	14.0	25.0	33.0	3.1	8.2	3.1	0.17	0.13	0.20	13.7	6.9	4.6
Winding pack	4	5000	26.1	26.9	41.1	5.75	10.4	10.5	0.26	0.20	0.20	14.7	14.0	14.0
	293	5000	21.0	22.3	38.4	4.31	8.10	8.55	0.29	0.17	0.17	14.7	14.0	14.0
AF coil ground insulation	4	3000	20.8	31.8	31.8	6.70	6.70	7.20	0.21	0.21	0.27	20.4	7.61	7.61
	293	3000	11.6	25.4	25.4	3.07	3.07	3.37	0.15	0.15	0.11	20.4	7.61	7.61
AF coil spacer G11Z	4	3000	24.0	36.0	36.0	8.90	8.90	11.6	10^{-3}	10^{-3}	10^{-3}	24.2	8.65	8.65
	293	3000	16.0	28.0	28.0	5.20	5.20	6.80	10^{-3}	10^{-3}	10^{-3}	24.2	8.65	8.65

Table 5
Initial gap width at narrow support element contact pairs.

Gap width [mm]	>2.0	2.0	1.5	1.0	0.5	0.2
Contact Element Description	npc1e2 npc1e6 npc1e7	npc1e3 npc1e10 npc4e4 pc5c1	npc2e5	npc1e5 npc1e9 npc2e6 npc3e5 npc3e6	npc1e12 npc2e9 npc3e4	npc1e4 npc1e11 npc2e7 npc2e10 npc2e11 npc3e10 npc3e11 npc3e12 npc4e8 npc4e9

Table 6
Coil load cases definition.

	Case	(B_0) [T]	I_1 [kA]	I_2 [kA]	I_3 [kA]	I_4 [kA]	I_5 [kA]	I_A [kA]	I_B [kA]
A	Standard	3.0	16.1	16.1	16.1	16.1	16.1	0.0	0.0
B	Low iota	3.0	14.7	14.7	14.7	14.7	14.7	11.0	11.0
C	High iota	3.0	17.8	17.8	17.8	17.8	17.8	−12.3	−12.3
D	Low mirror	3.0	15.1	15.8	15.8	17.1	17.1	0.0	0.0
E	High mirror	3.0	17.3	16.8	16.0	15.2	14.7	0.0	0.0
F	Low shear	3.0	18.2	17.9	16.9	13.7	13.5	−11.6	12.1
G	Inw. shift	3.0	15.7	15.5	15.8	17.5	17.6	4.9	−9.8
H	Outw. shift	3.0	16.9	16.9	16.4	15.6	15.6	−6.8	6.8
I	Limiter	3.0	17.0	17.5	16.2	14.6	14.1	−4.8	9.5

meshed independently with a much finer mesh. Modelling of such parts of the structure is shown in Figs. 11 and 12.

3.2. Material properties

The assignment of the different material properties to the particular structural part is given in Table 3.

The particular material properties definitions are presented in Table 4. All materials are linear elastic and defined by the elastic constants at 4 K and 293 K. In addition, all materials contract thermally from 293 K to 4 K. The orthotropic material properties define the complex compound structure of the coil winding packs.

3.3. Boundary conditions

In addition to the considerable number of contact surfaces used for the definition of the geometrical nonlinearity the model con-

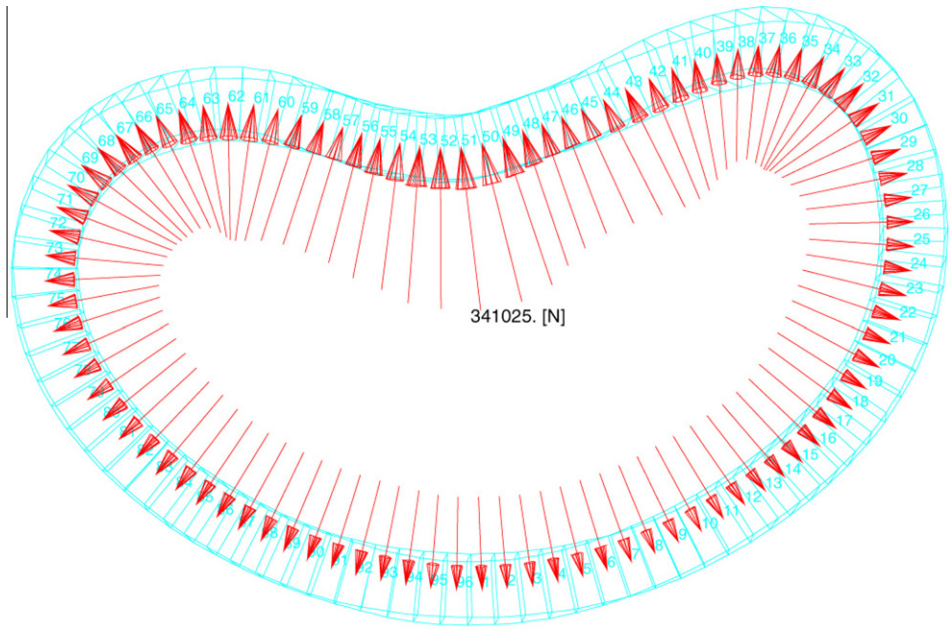

Fig. 13. Net coil force at coil type 1 – local radial component.

Table 7
Bolts pre-tension.

	Bolt	Shaft diameter [mm]	Pre-tension at 4 K [kN]
CSR-M-Flange	M42	34	625.0
CSR-HM-Flange	M42	34	630.0
CSR-HM-Flange (shear bolts)	M42	34	280.0
CSE	M30	27	~460.0
CSE	M90	80	3240.0
CSE	M76	65	2290.0
AF Coil A	M10	8	22.0
AF Coil B	M10	8	23.0

tains a large number of special boundary conditions. Essential for the behavior of the structure are the initial gaps at particular contact surface pairs. E.g. the initial gap width (Table 5) at narrow support elements contact pairs (27 within a half module) is essential for the stiffness of the whole structure.

For this contact group the initial gap width ranges from 0.2 to 4.5 mm dependent on the contact surface pressure and global displacements during operation.

An outline of the main boundary conditions and loading is given below.

3.3.1. Loading

The structure is loaded externally by electromagnetic forces caused by currents in the superconducting coils. Additional loading of the structure is due to weight and stresses caused by different thermal expansion coefficients during the cooling down. The coils are subjected to different so-called load scenarios. The currents for a flux density of B_0 = 3T at the plasma axis for different scenarios are summarized in Table 6. The magnetic forces are determined by means of the EFFI code [12] based on the Biot-Savart law (Eq. (1)):

$$f = j \times B \tag{1}$$

where f is the magnetic force density vector, j is the current density vector and B the vector of the magnetic induction.

The magnetic force density f for the use in ADINA code has been transformed into nodal forces using cubic isoparametric functions [13] shown in Eq. (2) for the corner nodes.

$$N_i = 1/32(1+\xi_0)(1+\eta_0)[-10+9(\xi^2+\eta^2)] \tag{2}$$

N_i denotes shape functions and ξ, η are nondimensional so-called normalized co-ordinates. An example of the electromagnetic force acting at one coil is shown in Fig. 13.

For the analysis shown in this paper the worst "Low Iota" load case (see Table 6) has been chosen.

The magnetic forces cause the mechanical stresses and strains in the coil system and the associated support structure. According to the sketches in Fig. 9 the coil winding pack is entirely embedded into the coil casing made of stainless steel. While the coil winding pack with the ground insulation and embedding layer build a continuum the casing is separated by a contact surface. Consequently, between the coil winding pack and the casing the compressive loads can be taken over only.

Due to the different local coil curvatures and the slightly helical arrangement of the coils, the force distribution within the system is inhomogeneous. For all five different coil types, the distribution of the magnetic force density is different. The variation of the radial component along the coil circumference for coil type one is shown in Fig. 13. The values of the magnetic force density vary over the coil cross-section as well. The volume integral of the magnetic force densities results in a net force on each coil. The moderate helicity of the magnetic axis causes a related helicity in the net coil force vector, corresponding to different coil forces in radial and vertical directions. All coils are affected by force components in the vertical direction which lead to a torque within each field period. For an entire field module, the horizontal net component force of about 10 MN is directed towards the torus centre and the vertical net component forces of about 7.0 MN vanish due to the symmetry conditions of the coil system. In this context, the special symmetry conditions described in [11] can be found by loads as folding-symmetry of 180° as well for each field module.

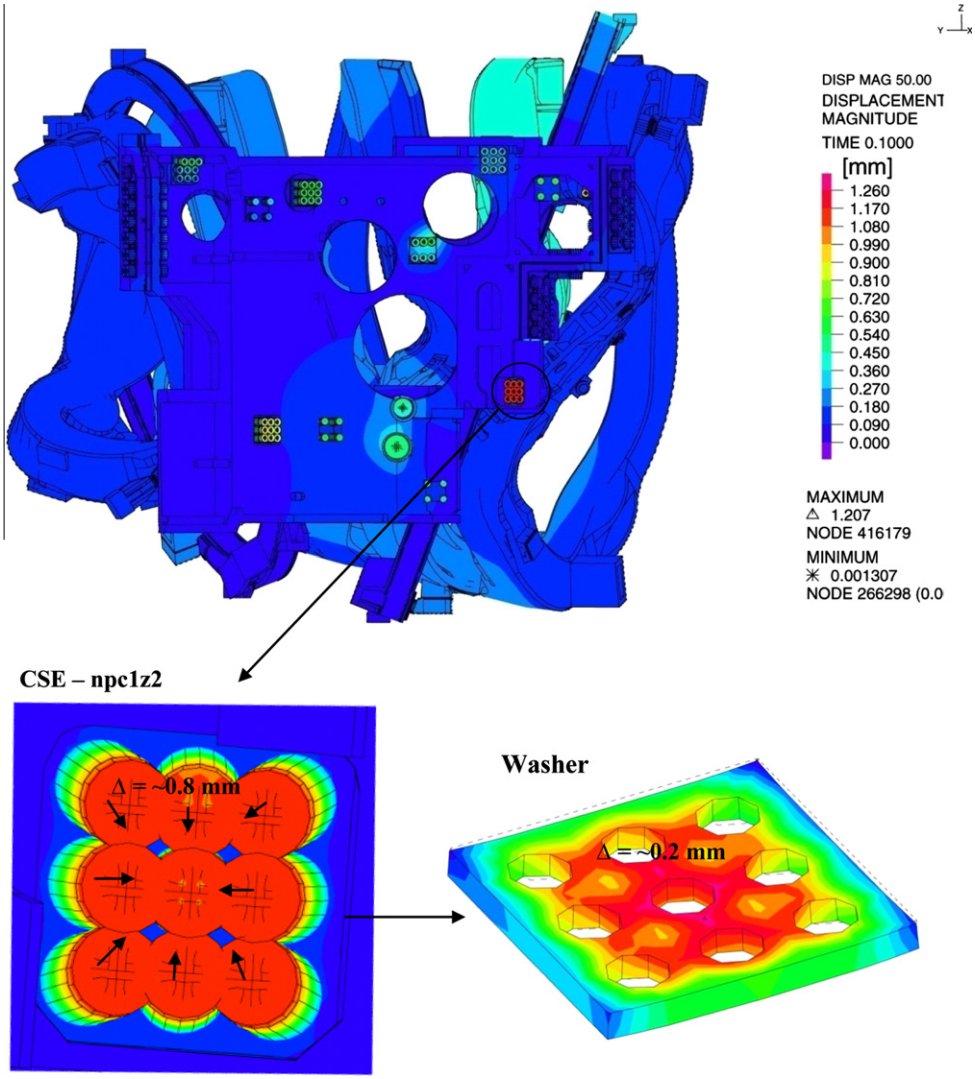

Fig. 14. Displacement after bolts pre-tension.

3.3.2. Bolts pre-tension

Inside of the structure there are approximately 950 bolts modeled with different dimensions and pre-tension values. Table 7 shows main bolts groups inside the structure with appropriate pre-tension values.

4. Results discussion

The problem solving and results evaluation have been performed by ADINA [14] code. Basically the whole analysis was performed by 8 node hexahedral elements model in the first place. Concerning the essential influence of the bolts pre-tension on the behavior of the structure during the operation, the analysis has been divided in two steps. In the first step, the forces at the bolts have been incrementally increased to the maximum and in the second step the electromagnetic forces at the coils have been superimposed gradually to the maximum as well. Correspondingly, the results evaluation is also split into two groups, the bolts pre-tension and the coil energising step. On the following pages, only the most important results of the stress-strain analysis are given.

4.1. Bolts pre-tension step

The displacements show that nearly the whole structure is already deformed after the bolts pre-tension. Especially the coil casing of the MF coil two shows quite high displacements, up to 0.5 mm. The reason is the long CSE of coil two which is squeezed by high bolts pre-tension. Fig. 14 shows the displacements of the whole structure viewed from the centre of the device.

A maximal displacement of typically ~1.2 mm appears at the heads of the long bolts. The extract in Fig. 14 shows that some bolt heads besides the main local axial displacement of about 1.2 mm also have a local lateral (small black arrows) displacement of about 0.8 mm. The local lateral displacements are caused by the deformation of the underlying washer (0.2 mm), respectively the CSE.

The contact surface pressure pattern at the half module (HM) flange of the central support ring shows a different pressure distribution over the contact surface caused by different bolts pre-tension (Fig. 15). The so-called shear bolts, introduced for the minimisation of the flange sliding, have lower pre-tension force to keep the bolts lateral contraction as low as possible. They produce areas with lower pressure.

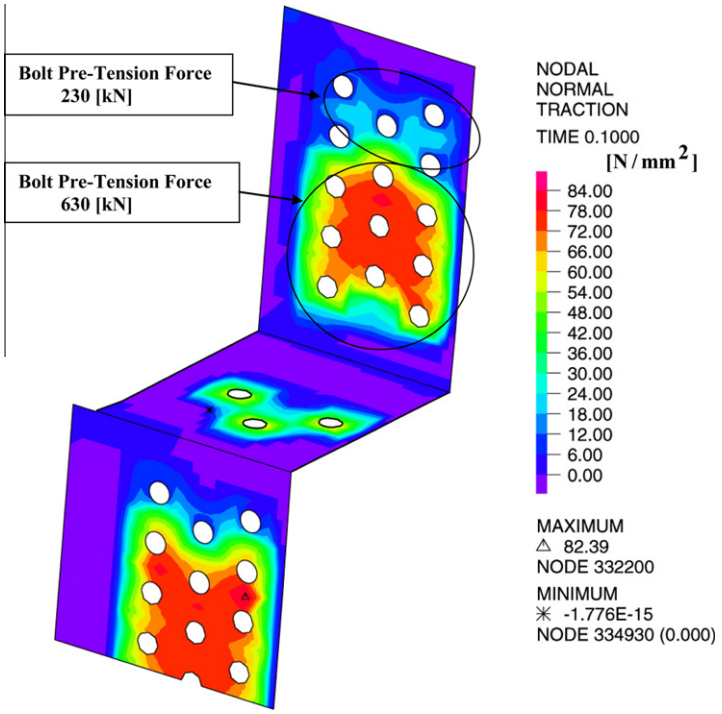

Fig. 15. Contact surface pressure at HM flange of the central support ring after bolts pre-tension.

A typical stress pattern of a structure under concentrated force action is shown in Fig. 16. The cross-section in this figure is located near the row of the 3 bolts at CSE "npc3z1". The band table values are limited to ±100.0 MPa, i.e. the stresses within the red zone are over 100 MPa until the maximum of about 1600 MPa. The local stress component σ_{11} shows that the whole cross-section of the extension is highly stressed already after bolts pre-tension.

4.2. Coil energising step

The first information about the behavior of the structure for a particular boundary condition case is given by the displacements. Fig. 17 shows the displacements of the whole structure in top view in case of the 8 node hexahedral elements model.

The high accuracy of the displacements evaluation for each part of the structure under operation conditions is highly important. A contact of structural elements close to each other might impede a proper operation of the superconducting coils.

The displacements gained by FE analysis have been transferred back to the CAD model for geometry morphing and subsequent collision analysis. Furthermore, the displacements for each main part of the structure were analysed separately. The displacements of the central support ring are shown in Fig. 18.

The main parts of the structure like the coil winding packs, the coil housings and the CSR are entirely designed regarding the standard allowable stresses. Fig. 19 shows the effective stress at the coil housings. Because of the better clearness the band table range in this figure is limited to 1000 MPa. The most stressed parts of the structure like the NSE, the CSE and the LSE were specially treated during the analysis and results evaluation. These elements have been subjected to special tests as well as numerous detailed local analyses. The global model results were taken as base for the additional analyses. A summary of these results is given below.

4.2.1. Cross-sectional loads

The weld seams which are exposed to high stresses were analysed locally [15]. The cross-sectional forces and moments gained through global analysis were used for these additional analyses [16–20].

The cross-sectional entities were evaluated in ADINA post-processing for cut surfaces like in Fig. 20 according to Eq. (3):

$$F = \int_V B^T \tau dV \tag{3}$$

where F is the nodal force, B is the element strain–displacement matrix and τ is the stress vector. The integration is performed over the volume of the element [21].

Table 8 shows an extract of the cross-sectional forces and moments for the CSEs referring to the element local coordinate system.

4.2.2. Results evaluation for NSE

Displacements of the whole structure are strongly dependent on the behavior of the NSEs during operation. The design of these elements is quite sophisticated because of the different operational conditions. Therefore, particular care was taken during the part modelling, the analyses, and the results evaluation for these elements. In order to make a precise results evaluation like contact surface pressure, surface area in contact and slipping possible, the NSE pads were modeled realistically with spherical surfaces.

Beside the required numerical analyses a lot of experimental tests have been performed. Figs. 21 and 22 show typical result presentations for the NSE contact surface traction and sliding. Table 9 represents a summary of the contact surface pressures.

In addition, relative tilting between the NSE contact pairs were analysed. This is very important due to possible edge overpressure which could damage the contact surface made of Al-bronze. Corresponding contact area results are shown in Fig. 23.

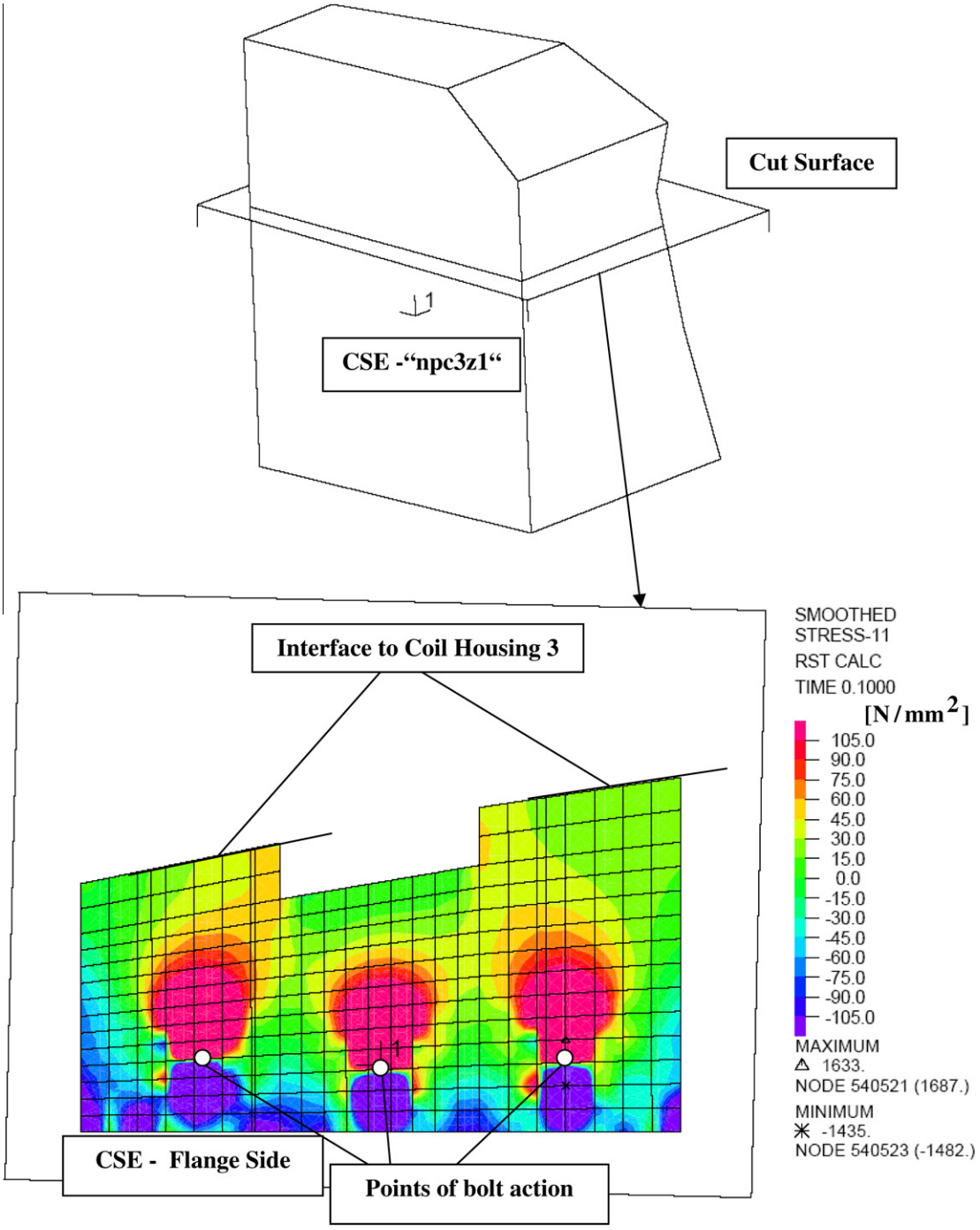

Fig. 16. In plane – local stress component σ_{11} at CSE "npc3z1" (State of stress after bolts pre-tension).

The plot shows a sufficient safety margin concerning the edge pressure for the current load case.

4.3. Results verification by 20 node hexahedral elements model

The 20 node hexahedral elements model was created with the aim to check the reliability of the result obtained by the FE model with 8 node hexahedral elements. Fig. 24 shows the displacements of the whole structure in top view in case of the 20 node elements FE model.

The comparison of the displacements for both of the models in Figs. 17 and 24 shows that the 20 node hexahedral elements model provides the displacement magnitude maximum at only 0.31 mm (~2.0%) higher than the 8 node hexahedral elements model. The displacement pattern over the whole structure and the maximum location remain nearly unchanged.

The stress plots show slightly higher differences, but only in regions with stress concentrations. In general these differences are covered by the safety margin for the stresses.

These results prove that the accuracy of the results of the 8 node global hexahedral elements model is sufficient.

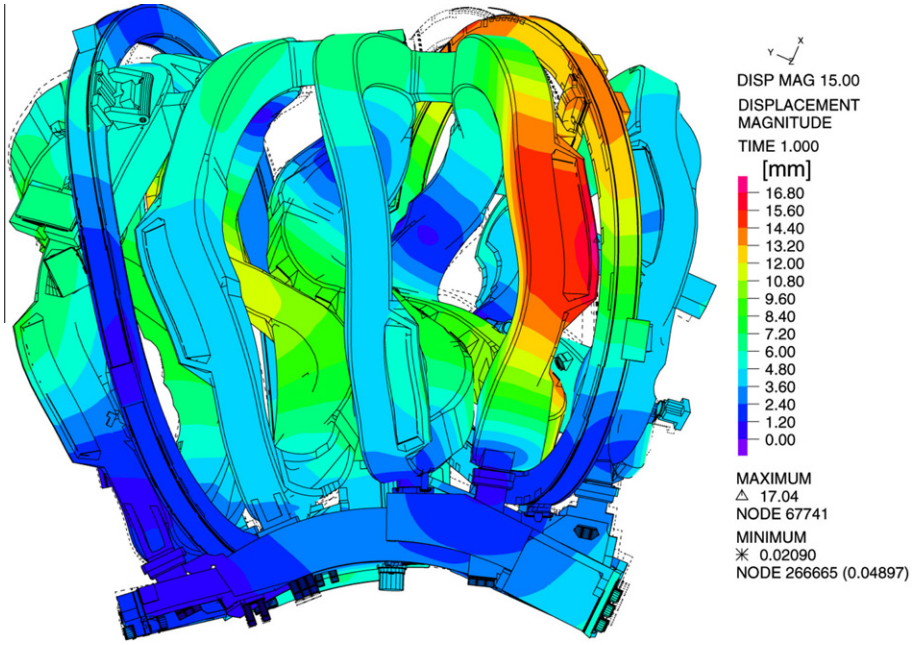

Fig. 17. Displacements magnitude of the whole structure – top view.

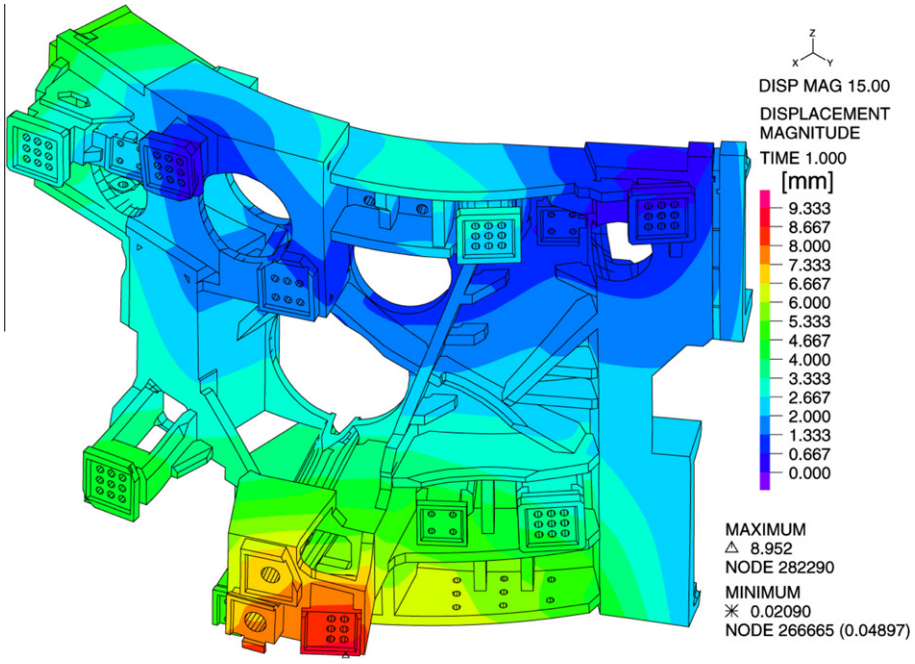

Fig. 18. Displacements magnitude of the central support ring – a bird's eye view.

5. ADINA analysis performance

The analyses of both of the models, the 8 node and the 20 node hexahedral elements model have been performed using an IBM, AIX 5.1, 64-bit computer. This is a parallel processing machine with 30 POWER6 CPUs and 124 GB RAM memory.

The ADINA sparse matrix solver with full Newton iteration scheme has been used for the analyses in both cases. Both, the energy and the displacement convergence criteria have been used in the solution process. The contact force tolerance criterion is always active if the contact algorithm is used. Table 10 shows typical ADINA performance characteristics for both models.

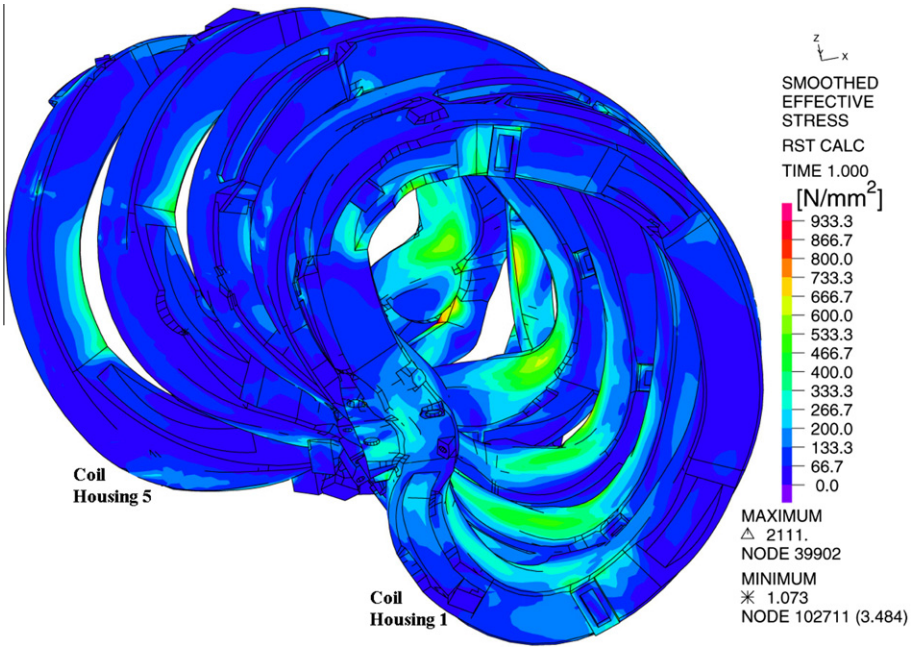

Fig. 19. Von Mises stress at MF coil housings – view on the most stressed area.

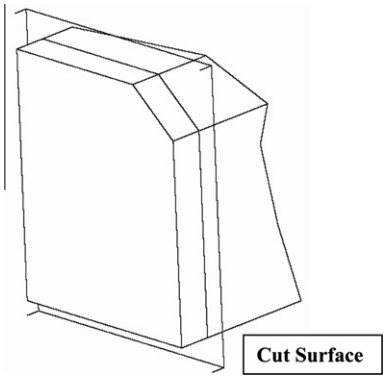

Fig. 20. Cut surface definition for CSE "npc3z1".

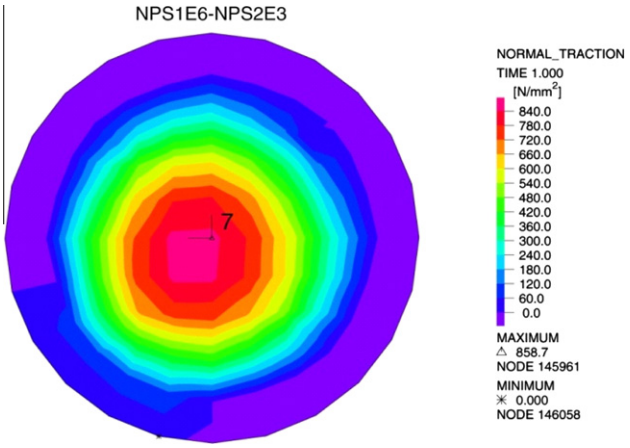

Fig. 21. Contact surface pressure.

Table 8
Cross-sectional forces and moments at CSE.

CSE-ID		Fx [MN]	Fy [MN]	Fz [MN]	Mx [MNmm]	My [MNmm]	Mz [MNmm]
NPC1	Z1	0.60	0.24	1.10	0.104	0.274	-0.012
	Z2	−2.74	0.22	−0.54	0.010	−0.153	−0.098
NPC2	Z1	−0.60	−0.36	0.80	0.130	0.195	−0.089
	Z2	−0.75	0.03	−1.02	0.025	−0.207	−0.087
NPC3	Z1	−0.90	0.10	0.65	0.126	0.098	0.034
	Z2	−1.90	0.53	−0.87	0.027	−0.138	−0.160
NPC4	Z1	0.10	−0.02	−0.81	0.014	−0.062	−0.005
	Z2	−2.10	0.12	−0.80	−0.051	−0.116	−0.013
NPC5	Z1	0.06	−0.65	−0.38	−0.025	−0.062	−0.065
	Z2	1.70	−0.11	−0.13	0.031	−0.006	0.014
PLCA	Z1	0.14	−0.02	−0.17	0.008	0.035	−0.008
	Z2	−0.07	−0.07	0.19	0.016	0.010	−0.015
PLCB	Z1	0.08	0.02	−0.11	0.008	0.003	−0.009
	Z2	0.04	0.05	−0.01	−0.004	−0.018	0.008

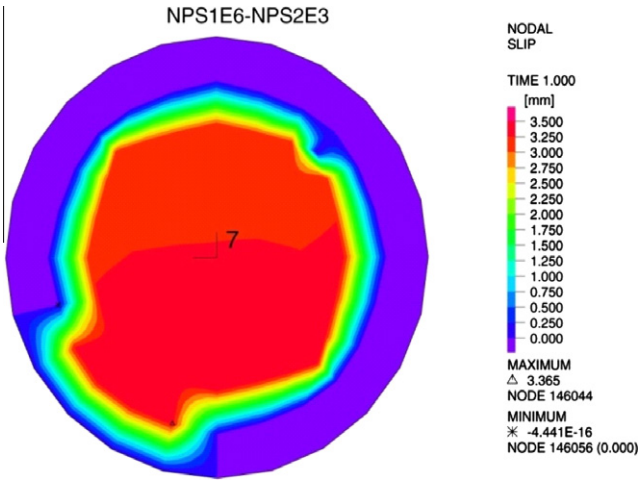

Fig. 22. Contact surface sliding.

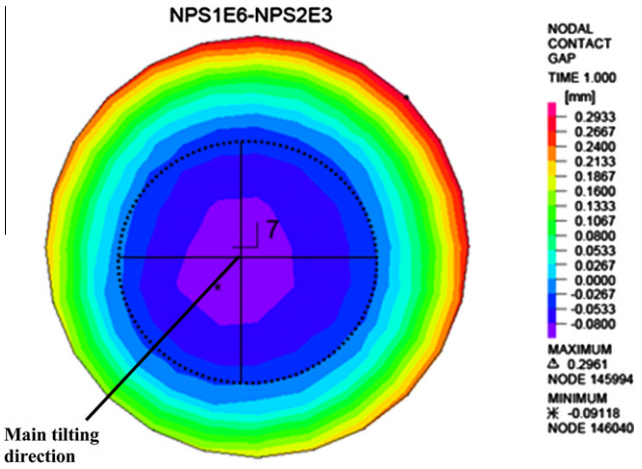

Fig. 23. Surface area in contact – dashed line.

6. Conclusions

The presented ADINA FE model for the structural analysis of the W7-X superconducting magnet coil system is the result of a long term R&D activity. This work was particularly challenging because the W7-X device is in many respects a one of a kind prototype worldwide.

During the development phase, starting at the very beginning of the project, at least three quite different coil support structure alternatives have been iteratively analysed. One of the difficulties was due to the fact that a decision about a suitable concept could not be made before going into structural details at the lowest level.

The presented coil support structure unifies the experience gained in over 18 years work on the W7-X project with all its technical, economical and time constraints. The final ADINA FE model contains all essential features for a greatest reasonable global analysis precision. It was not always possible to confirm the desired safety factor for each individual part of the structure; some critical components have to be operated at their limits. Therefore, in order to corroborate the reliability of these elements and the whole support structure, they were subjected to numerous additional local analyses and mock-up tests, and are well instrumented for monitoring during operation.

The present structural analysis of the magnet system, which is independently performed also with ANSYS and ABAQUS FE codes, is mainly concentrated on accompanying the machine construction by evaluating specific assembly issues, non-conformities and design changes, but also on ensuring the device reliability by finding out the operational limits.

The valuable knowledge from the here presented analysis procedure is that the FE models with the complexity similar to the W7-X global model of the magnet system should be benchmarked with independent alternative models of the same quality. Besides of the studies of model reliability and sensitivity the benchmarking process is extremely important. During benchmarking between three independent FE models more than 30 errors have been found and fixed in parameters, boundary conditions and post-processing routines.

The comparison of the results of the benchmark analysis shows a maximum deviation of 2.0 mm for displacements with a maximum value of 18.7 mm. Furthermore, the comparison of the cross-sectional forces and moments and the comparison of the contact forces show sufficient agreement. All results of the benchmark analysis show values within the expected limits, i.e. they are within 10% for the critical components and 30% for the non-critical ones.

These limits for different load scenarios (i.e. field configurations) and 3 T at the plasma axis have to be approached with utmost care. However, the nominal field of 2.5 T at the axis which allows all planned plasma physics experiments can be safely achieved.

For the preparation of the ADINA FE model for this complex and geometrically multiple nonlinear structures, the PATRAN code was an indispensable tool. From the beginning of all these developments the ADINA staff (Boston, USA) provided very valuable support by solving special issues.

According to the present plan, the W7-X experimental device shall have its first plasma in the year 2015.

Table 9
Contact surface pressure at NSEs.

Contact surface pressure [MPa]	>800 Max. 855	700–800	600–700	500–600	400–500	0–400
Contact element description	npc1e6 npc2e4 npc2e5 npc2e11 npc3e10	npc1e2 npc1e8	npc1e3 npc1e5 npc2e6 npc2e8 npc3e3 npc3e7 npc3e8	npc2e9 npc4e1 npc4e3 npc5e3	npc2e10	npc1e4 npc4e2 npc4e6 npc247 npc5e5 npc5e

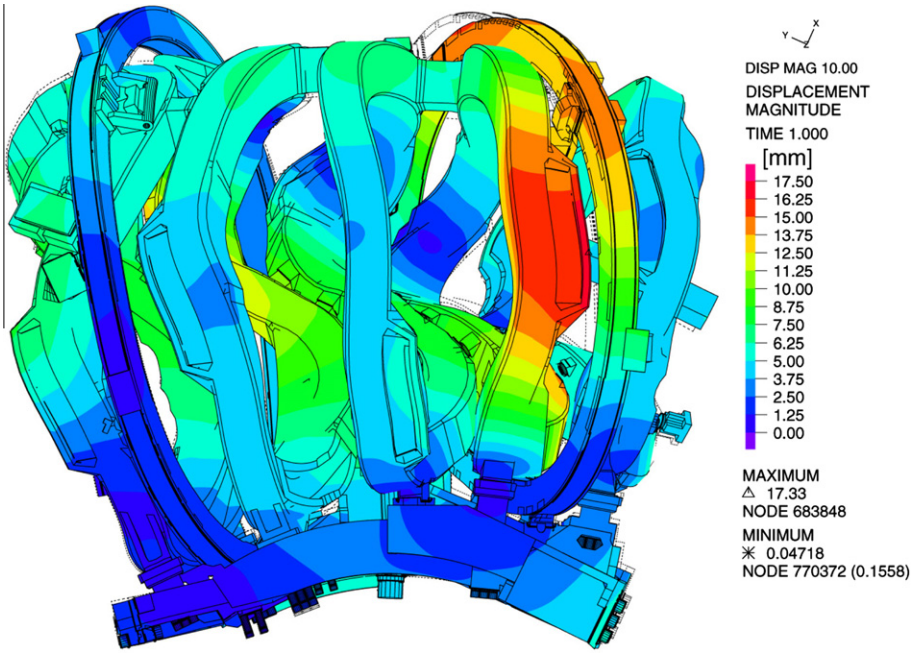

Fig. 24. Displacements magnitude of the whole structure – top view.

Table 10
The main ADINA performance characteristics.

	8 node hexahedral elements model	20 node hexahedral elements model
Number of processors used	28	28
Memory used by the in-core sparse solver [GB]	5.7	43.4
Total memory used by the program [GB]	8.0	52.3
Total number of equations	1688991	5865765
Number of contact equations	210857	698579
Total solution time [s]	13359	208708

Acknowledgements

The authors thank Mr. J. Tretter for his valuable discussion and the help during the preparation of this paper.

References

[1] Nührenberg J et al. Overview on Wendelstein 7-X theory. Trans Fusion Technol 1995;27:71–8.
[2] Grieger G et al. Physics optimisation stellarators. Phys Fluids 1992;B4: 2081–91.
[3] Jaksic N, et al. Support system for the W7-X coil assembly. In Proc 20th SOFT. Marseille, France, September 7–11; 1998. pp. 819–22.
[4] Jaksic N et al. Nonlinear global-local finite element analysis of a future plasma fusion experiment. Comput Struct 1999;72:209–31.
[5] Jaksic N et al. Design analysis of the support structure stressed by large superconducting coils for a plasma fusion experiment. Comput Struct 2003;81: 697–714.
[6] Bykov V, et al. Strategy of structural analysis of W7-X magnet system. In Proc 21 IEEE/NPS Symposium on Fusion Engineering 2005 (CD-Rom). IEEE 2006, paper 04_11.
[7] Bykov V, et al. Main results and critical issues of W7-X structural analysis. In Proc 22 IEEE/NPS Symposium on Fusion Engineering 2007. IEEE 2007, ISBN: 978-1-4244-1194-8.
[8] Schauer F, et al. Status of Wendelstein 7-X construction. In 24th SOFT Symposium on Fusion Technology. Warsaw, September 11–15; 2006.
[9] Eeten van P, et al. Design and test of the support elements of the W7-X superconducting magnets. In 22nd SOFE Symposium on Fusion Engineering 2007. IEEE 2007, ISBN: 978-1-4244-1194-8.
[10] MSC.PATRAN 2005 r2, A finite element modeler, MSC. Software Corporation, 2 MacArthur Place Santa Ana, California 92707; 2008.
[11] Jaksic N, et al. Defnition der Randbedingungen bei einer FE-Strukturanalyse durch Nutzung der Symmetriebedingungen einer Stellaratoranordnung, IPPZ/ 3; February 1997.
[12] Sackett SJ. EFFI––a code for calculating the electromagnetic field, force, and inductance in coil systems of arbitrary geometry. Lawrence Livermore National Laboratory, Report UCRL-52402; March 1978.
[13] Zienkiewicz OC. The finite element method in engineering science. London: McGraw-Hill; 1971. p. 106–9.
[14] AD INA R&D Inc., A finite element computer program for Automatic Dynamic Incremental Nonlinear Analysis – System 8.5. 71 Elton Avenue, Watertown, MA 02472 USA; February 2008.
[15] Fellinger J, et al. Weld integrity of the superconducting cable aluminium jackets of W7-X. Fusion Eng Des; 2009. doi:10.1016/j.fusengdes.2009.01.037.
[16] Hathiramani D, et al. Full scale friction test on tilted sliding bearings for Wendelstein 7-X coils. Fusion Eng Des; 2008. doi:10.1016/j.fusengdes.2008.11.084.
[17] Dudek A, et al. Verification tests of critical bolted connections of the W7-X coils. Fusion Eng Des; 2008. doi:10.1016/j.fusengdes.2008.11.032.
[18] Krzesinrski G et al. FEM analysis of coil support connections in the Wendelstein 7-X magnet system. Fusion Eng Des 2007;82:1574–8.
[19] Ciupinrski Ł, et al. Evaluation of the structural mechanical behavior of W7-X central support connections by means of semi-automated FE analysis. Fusion Eng Des; 2009. doi:10.1016/j.fusengdes.2009.02.011.
[20] Czarkowski P. Structural analysis of the central support elements for the Wendelstein 7-X magnet system. Fusion Eng Des; 2009. doi:10.1016/ j.fusengdes. 2009.02.012.
[21] Bathe KJ. Finite element procedures. Upper Saddle River, NJ: Prentice-Hall; 1996.